

Design and Reconstruction the Digital Holography Microscopy

تصميم واعادة بناء مجهر الهولوكرافي الرقمي

Rafah Abdul Hadi Omer, Khawla Jameel Tahir, Sarah Abdul Hussein Ali
Department of Physics, College of Science for Women, \University of Baghdad .

Abstract

In-line DHM was designed, holograms recorded and the numerical reconstructions were made using an algorithm based on the diffraction theory in Fresnel approximation using Fourier Transformation. Using double Nd:YAG laser ($\lambda = 532$ nm) output (approximately 30 mW), and CCD camera used with 1024 X 1024 pixels , microscopic objective with 0.87 NA was used for magnification, obtained images resolution about $0.31\mu\text{m}$. we observed there are Inverse relationship between the numerical aperture and the resolution .

for applying this new microscope we used it for a biological sample -red blood cells- that took it from different diseases (e.g. *Healthy Person, G6PD, Thalassemia Major ,SCD ,Hereditary Spherocytosis*) and making a blood films from it , We present the experimental image result, their 3D image, cross section profiles and histogram. these offer insight into the nature of morphological abnormalities used to identify various disorders, to compute important parameters for each cells have morphological changes (*Normal Cell , Anchitocyte , Bite Cell, Elliptocyte, Macrocyte , Spherocyte , Sickle Cell , Stomatocyte , Target Cell , Tear Drop Cell*) in this easy way this parameters like Diameter ,Thickness ,Refractive Index , Optical Path Length, Surface Area , Volume ,Spherocity Index.

We found that the diameter of the cells limit between ($9.9\mu\text{m}$ for macrocyte - $3.9\mu\text{m}$ for sickle cell) and the normal cell was $7.4\mu\text{m}$, and the thickness of the cells limit between ($2.249\mu\text{m}$ for Tear-drop cell - $4.233\mu\text{m}$ for Spherocyte) and the normal cell was $2.646\mu\text{m}$. refractive index values of 1.18 to 2.22 were and 2.64 for normal cell. The surface areas of individual erythrocytes were measured range from $251.1\mu\text{m}^2$ for macrocyte to $70.8\mu\text{m}^2$ for sickle cell and the normal cell was $147.70\mu\text{m}^2$,and The volumes of individual erythrocytes were calculated range from $239.25\mu\text{m}^3$ for macrocyte to $45.8\mu\text{m}^3$ for sickle cell and the normal cell was $113.98\mu\text{m}^3$

Keywords : Digital Holographic Microscopy , In-Line DHM, Fresnel approximation , Red Blood Cells.

المخلص

تم تصميم المجهر الرقمي ثلاثي الابعاد DHM باستخدام الطريقة المحورية وتمت عملية تسجيل الهولوكرام في المختبر و اعادة البناء العددي باستخدام خوارزمية على أساس نظرية الحيود لفرينسل باستخدام معادلات فورير . باستعمال الليزر النديميوم : ياك مضاعف التردد ذو الطول الموجي 532 نانومتر وقدرة اخراج (حوالي 30 ملي واط) ، و كاميرا رقمية CCD مع 1024 X 1024 بكسل ، و تم استخدام الفتحة العددية قيمتها 0.87 للتكبير ، وتم الحصول على قدرة التحليل بمقدار 0.31 مايكرو متر. ولاحظنا ان هناك علاقة عكسية بين قيمة الفتحة العددية و قيمة قدرة التحليل.

بعد ذلك تم تطبيق المجهر على مجموعه من العينات بيولوجية - كريات الدم الحمراء - نتيجة اصابتها بأمراض (e.g. *Healthy Person, G6PD, Thalassemia Major ,SCD ,Hereditary Spherocytosis*)

تمت معرفه التشوهات التي تصيب هذه كريات الدم الحمراء (*Normal Cell , Anchitocyte , Bite Cell, Elliptocyte, Macrocyte , Spherocyte , Sickle Cell , Stomatocyte , Target Cell , Tear Drop Cell*)

من خلال الصورة الثلاثية الابعاد، المقطع العرضي والهستوكرام. فأن هذا طريقة سهلة لحساب المعلومات الهامة لكل الخلايا التي لديها تغيرات شكلية مثل القطر، و سمك، و معامل الانكسار، و طول مسار بصري، مساحة السطح، و حجم، مؤشر الكروية.

وبذلك وجدنا أن قطر الخلايا منحصرة بين (3.9-9.9) مايكرومتر وكان الخلية العادية 7.4 مايكرومتر ، وسمك الخلايا منحصرة بين (2.249 - 4.233) مايكرومتر و الخلية العادية 2.646 مايكرومتر. تم قياس المساحات السطحية من الكريات الحمراء تتراوح من (70.8-251.1) مايكرومتر مربع و كانت الخلية الطبيعية 147.70 مايكرومتر مربع ، و تم حساب حجم كريات الدم الحمراء من 239.25 إلى 45.8 مايكرومتر مكعب و كان الخلية العادية 113.98 مايكرومتر مكعب.

1. Introduction

Digital holographic microscopy (DHM) is a powerful instrument for the study of microscopic samples by retrieving the amplitude and phase of the wave reflected by the sample or transmitted through it [1] .

Modern medicine and therapy rely on early and precise diagnosis to permit localized and specific treatments. Three-dimensional (3D) imaging of complex microscopic and submicroscopic processes in tissues, down to the cellular level, is still a challenging issue. Rapid, sensitive, non-invasive methods with high-resolution capability are thus needed for diagnosis of lesions or tissue dysfunctions. Digital Holographic Microscopy (DHM) offers new opportunities likely to fulfill these requirements. In DHM the hologram is recorded on a Charge Coupled Device (CCD) camera and reconstructed numerically on a PC, giving direct access to the phase and amplitude of the reconstructed wavefront, with a high vertical accuracy in the nanometer range and a diffracted limited transverse resolution [2] .

The main advantages of DHM is that only a single hologram is needed for each orientation of the specimen, leading to short acquisition time and low stability requirements for the system. The biological specimen observed is red blood cell (RBC), having a 3D-structured nucleus, which makes it an ideal test specimen for the method [3] .

MATURE erythrocytes represent the main cell type in circulating blood. They can be characterized by specific biconcave shape, high hemoglobin content, and absence of intracellular organelles Fig.1. Parameters such as RBC shape and refractive index are important characteristics that can be considers as good indicators of the body's physiological state[4] .

The aim of this paper is to design and reconstruction the digital holography microscopy offer insight into the nature of morphological abnormalities used to identify various disorders.

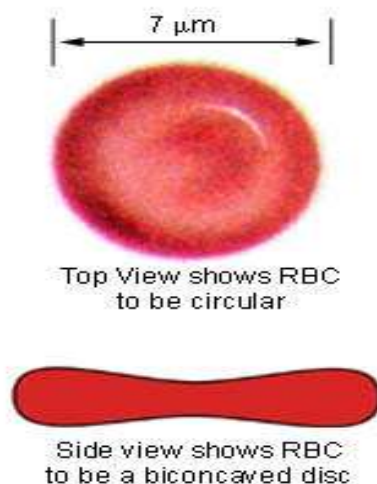


Fig. 1 RBC shap+

2. Principles Of Digital In-Line Holographic Microscopy

The holographic process takes place in two stages: the recording of an image, and the reconstruction [5] .

The intensity of the light incident on the recording medium can be written as the sum of two wavefields

$$h(x, y) = R(x, y) + O(x, y) \dots\dots\dots (1)$$

where $R(x, y)$ is the amplitude of the reference wavefield, $O(x, y)$ is the amplitude of the object wavefield. The real-valued intensity $|h(x, y)|^2$ is recorded and may be written as

$$I(x, y) = |h(x, y)|^2 = |R(x, y)|^2 + |O(x, y)|^2 + R^*(x, y) O(x, y) + O^*(x, y)R(x, y) \dots\dots\dots (2)$$

where $I(x, y)$ is the intensity, * denotes the complex conjugate, $R^*(x, y) O(x, y)$ and $O^*(x, y)R(x, y)$ are the virtual and real image terms, and $|R(x, y)|^2$ and $|O(x, y)|^2$ are the DC terms (which includes reference and object field intensities). As the third term, $R^*(x, y) O(x, y)$, is proportional to the object wavefield, $O(x, y)$, it produces a virtual image of the object. Consequentially the fourth term, $O^*(x, y)R(x, y)$, which is proportional to the conjugate of the object wavefield, produces a real image see fig. 2 [6] .

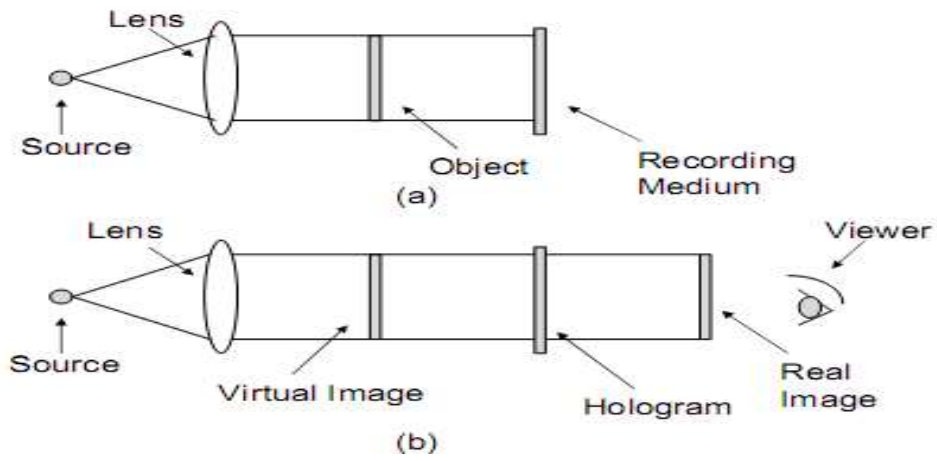


Fig 2. The capture (a) and reconstruction (b) of a Gabor hologram.

3. Theory

3.1 Numerical Calculation

There are a number of different methods developed for numerically calculating the diffraction field. More common approaches in digital holography have been the Fresnel transform and Huygens convolution methods, as well as, more recently, the angular spectrum method . These methods are closely related to each other, and the terminology is not uniform [7] .

Once the hologram has been recorded, it remains to reconstruct the optical field by computationally simulating diffraction using one of these numerical methods .

In this section we review the numerical reconstruction of a DHM. We recall that $|h(x, y)|^2$ is the intensity recorded by the CCD. It is formed when the object wave $O(x, y)$, after propagation a distance d , interferes with the reference wave $R(x, y)$.

We also recall that the intensity term is made up of the sum of four terms, the object and reference terms and the real and virtual images. The image plane (reconstructed DHM) is a distance d from the hologram (CCD) plane.

Numerical reconstruction produces a discretely sampled complex distribution $recon(m_x, T_x, m_y, T_y)$ representing the reconstructed image, where m_x and m_y are integer indices and T_x and T_y are the sampling intervals in the reconstruction plane (x', y') . A number of different algorithms exist to numerically reconstruct a digital hologram, and obtain values for

$recon(m_{x'} T_{x'}, m_{y'} T_{y'})$. These different algorithms have different values for $T_{x'}$ and $T_{y'}$. Fresnel transformation method is used in the present research[8].

Fresnel transform method:

The Fresnel transformation is the most commonly used method in holographic reconstruction. The direct method is briefly derived as follows; We begin by applying the Fresnel Transform to the sampled signal $O(n_x T_x, n_y T_y)$ which denotes the sampled object term in the hologram (CCD) plane to obtain an equation for the continuous reconstructed image $recon(x', y')$.

$$recon(x', y') = \frac{\exp[ikd]}{j\lambda d} \exp\left[\frac{j\pi}{d\lambda}(x'^2 + y'^2)\right] \dots \times \iint O(n_x T_x, n_y T_y) \exp\left[\frac{j\pi}{d\lambda}(x^2 + y^2)\right] \times \exp\left[\frac{j\pi}{d\lambda}(x' + y')\right] \dots \dots \dots (3)$$

The constant $\frac{\exp[ikd]}{j\lambda d}$ does not depend on the spatial frequency coordinates or the object and so can be omitted. We note that since the signal O exists only at discrete spatial coordinates, only these discrete values of x and y need to be considered in the above integral;[9]

$$x = n_x T_x \qquad n_x = -\frac{N_x}{2}, \dots, \frac{N_x}{2} \dots \dots \dots (4 - a)$$

$$y = n_y T_y \qquad n_y = -\frac{N_y}{2}, \dots, \frac{N_y}{2} \dots \dots \dots (4 - b)$$

where T_x and T_y are the CCD pixel pitch in the x and y directions respectively, and where N_x and N_y are the number of pixels in the CCD camera in the x and y directions respectively. We can conclude that W_{CCDx} and W_{CCDy} , the widths of the camera in the x and y directions are given by $N_x T_x$ and $N_y T_y$ respectively.[10]

then Equation 1 reduces to

$$x' = m_{x'} T_{x'} \qquad m_{x'} = -\frac{N_x}{2}, \dots, \frac{N_x}{2} - 1 \quad (5 - a)$$

$$y' = m_{y'} T_{y'} \qquad m_{y'} = -\frac{N_y}{2}, \dots, \frac{N_y}{2} - 1 \quad (5 - b)$$

then Equation 3 reduces to

$$recon(m_{x'} T_{x'}, m_{y'} T_{y'}) = \frac{\exp[ikd]}{j\lambda d} \exp\left[\frac{j\pi}{d\lambda}((m_{x'} T_{x'})^2 + (m_{y'} T_{y'})^2)\right] \times \sum_{n_x=-\frac{N_x}{2}}^{\frac{N_x}{2}-1} \sum_{n_y=-\frac{N_y}{2}}^{\frac{N_y}{2}-1} O(n_x T_x, n_y T_y) \times \exp\left[\frac{j\pi}{d\lambda}((n_x T_x)^2 + (n_y T_y)^2)\right] \times \exp\left[\frac{j\pi}{d\lambda}(m_{x'} T_{x'} n_x T_x + (m_{y'} T_{y'} n_y T_y))\right] \dots \dots \dots (6)$$

If we choose the output sampling intervals to be defined as follows[11]

$$T_{x'} = \frac{\lambda d}{N_x T_x} = \frac{\lambda d}{W_{CCDx}} \dots \dots \dots (7 - a)$$

$$T_{y'} = \frac{\lambda d}{N_y T_y} = \frac{\lambda d}{W_{CCDy}} \dots \dots \dots (7 - b)$$

$$recon(m_{x'} T_{x'}, m_{y'} T_{y'}) = \frac{\exp[ikd]}{j\lambda d} \exp\left[\frac{j\pi}{d\lambda}((\lambda d m_{x'} T_x)^2 + (\lambda d m_{y'} T_y)^2)\right] \times$$

$$\sum_{n_x=-\frac{N_x}{2}}^{\frac{N_x}{2}-1} \sum_{n_y=-\frac{N_y}{2}}^{\frac{N_y}{2}-1} O(n_x T_x, n_y T_y) \exp \left[\frac{j\pi}{d\lambda} ((n_x T_x)^2 + (n_y T_y)^2) \right] \times \exp \left[j2\pi \frac{n_x m_{x'}}{N_x} + j2\pi \frac{n_y m_{y'}}{N_y} \right] \dots \dots \dots \quad (8).$$

This equation can be calculated using the very time efficient FFT algorithm. We note that the output window size in the x' and y' dimensions can be calculated to be

$$N_x T_{x'} = \frac{\lambda d}{T_x}, \quad \dots \dots \quad (9 - a)$$

$$N_y T_{y'} = \frac{\lambda d}{T_y} \quad \dots \dots \quad (9 - b)$$

It is clear that the output window size is directly proportional to the distance of propagation, d, and inversely proportional to the sampling interval Tx and Ty in both dimensions.[9]

The resultant field $recon(m_{x'} T_{x'}, m_{y'} T_{y'})$ is the numerical representation of a complex optical wavefield and from it the intensity $Image(m_{x'} T_{x'}, m_{y'} T_{y'})$ and the phase $\phi(m_{x'} T_{x'}, m_{y'} T_{y'})$ can be determined as

$$Image(m_{x'} T_{x'}, m_{y'} T_{y'}) = |recon(m_{x'} T_{x'}, m_{y'} T_{y'})|^2, \quad \dots \dots \quad (10)$$

$$\phi(m_{x'} T_{x'}, m_{y'} T_{y'}) = \tan^{-1} \left(\frac{Im\{recon(m_{x'} T_{x'}, m_{y'} T_{y'})\}}{Re\{recon(m_{x'} T_{x'}, m_{y'} T_{y'})\}} \right) \dots \dots \quad (11)$$

respectively, where Im{ } represents the imaginary part and Re{ } the real part of the resultant field $recon(m_{x'} T_{x'}, m_{y'} T_{y'})$ [11].

4. Methodology

4.1 Samples Preparation :

The preparation of blood samples are performed by taking a blood specimen with normal and abnormal cells take from different diseases (healthy person, G6PD, Thalassimia major ,SCD, Megaloblastiosis and hereditary spherocytosis) were prepared for diagnosis under the DHM.

there are three step of making a blood films as it show in figure 3 they are:

1. preparation of blood smear see (3-a) .
2. fixation of blood smear by air see (3-b).
3. staining of blood smear by Lishman stain see (3-c and d).

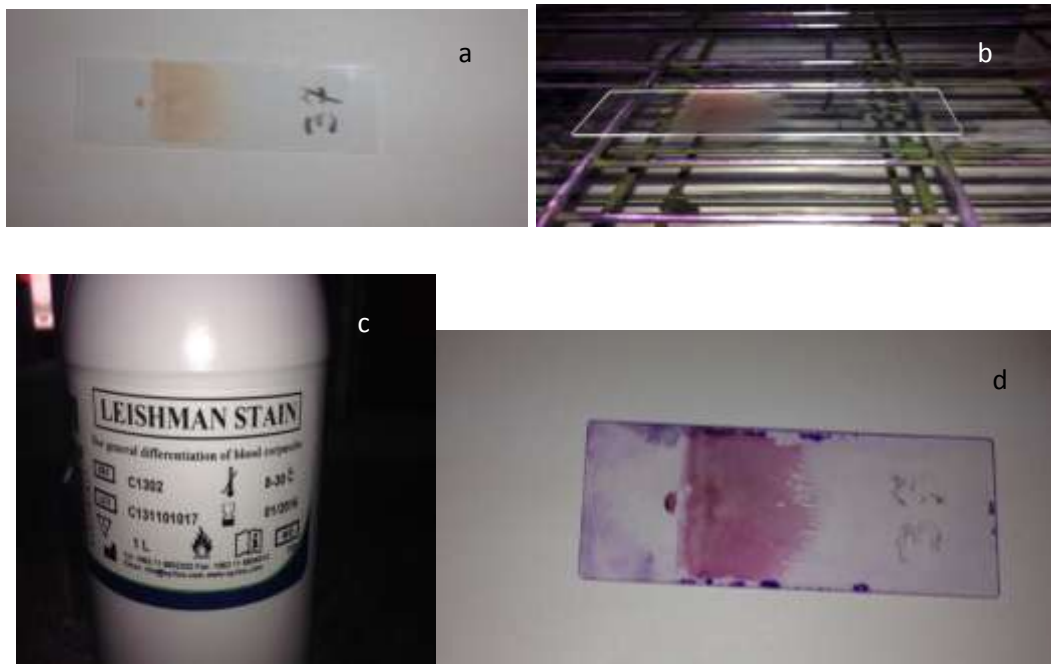


Figure 3. Preparing blood film

4.2 Experimental Set Up

Digital in-line holography has come to represent a new tool for biological applications, The hardware required is a laser, microscope objective , and a CCD camera.

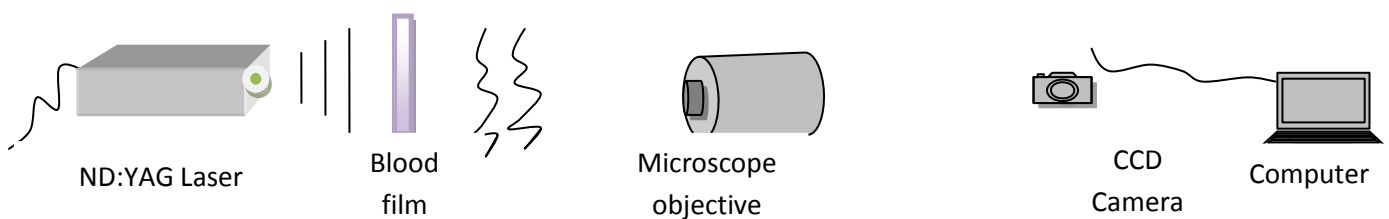


Figure 4. show the experimental set-up for a digital in-line holographic microscope. The blood film is illuminated by one beam .A microscope objective collects the transmitted light and forms the object wave, which interferes with a reference beam to produce the hologram recorded by the digital CCD camera.

The digital holographic microscope (DHM) that we have developed is in-line digital holography microscopy .The experimental setup is schematically depicted in Fig. 4. The specimen is illuminated by a frequency double Nd:YAG laser ($\lambda = 532 \text{ nm}$) and the transmitted light is collected by a 100X microscope objective with 0.87 NA The numerical aperture (NA) refers to the amount of light that which enters the objective. And The resolution is 0.31 that produces a wave front called object wave, The CCD camera(sony) (1024×1024 pixels) records -Holograms - the interference of this object wave with a reference plane wave fig 5.



Figure 5 Photograph for Setup of The DHM.(Karbala University ,College Of Science)

Numerical reconstruction of holograms were performed on a laptop ASER ASPIRE V5-571 series with an Intel P8400 Core i3 processor of clock speeds of 2.26 GHz per processor with 1 GB of RAM. and MatLab 7.14.0.739 (R2012a) (Mathworks Inc).

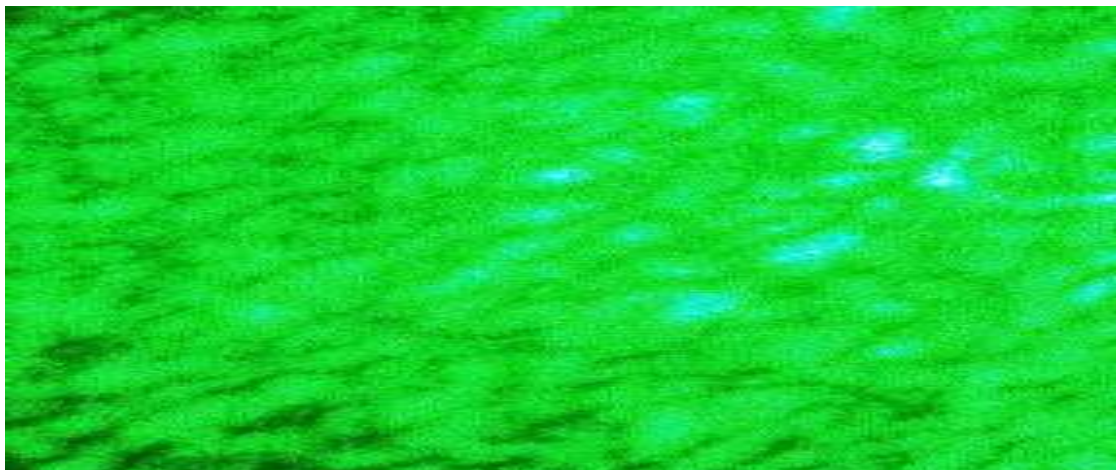


Figure 6. this picture represent the result of recording process its the Digital hologram for blood film from Thalassemia Major Diseases which contains a several abnormal shape for RBC's like target cell and tear drop cell

5. Results and discussion

The recording hologram was reconstructed by using Fresnel propagation; the program was designed using Matlab

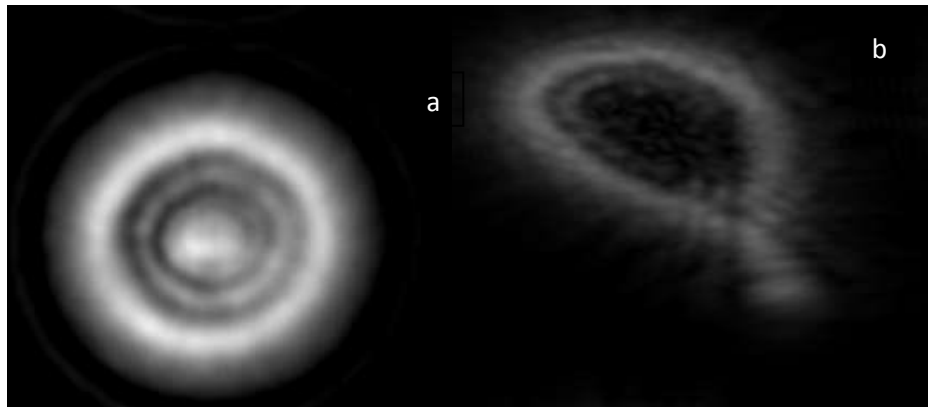


Figure 7 Experimental results obtained with RBCs image with for a- target cell b- tear drop cell. After reconstruction using MATLAB program

three dimensional image show that target cell in figure 8. A. are abnormal red blood cells, They show a shallow but visible round depression in the central portion of the cell, which in turn is surrounded by a peripheral hemoglobinized zone. tear drop in b. Red cells appearing in the shape of a tear drop.

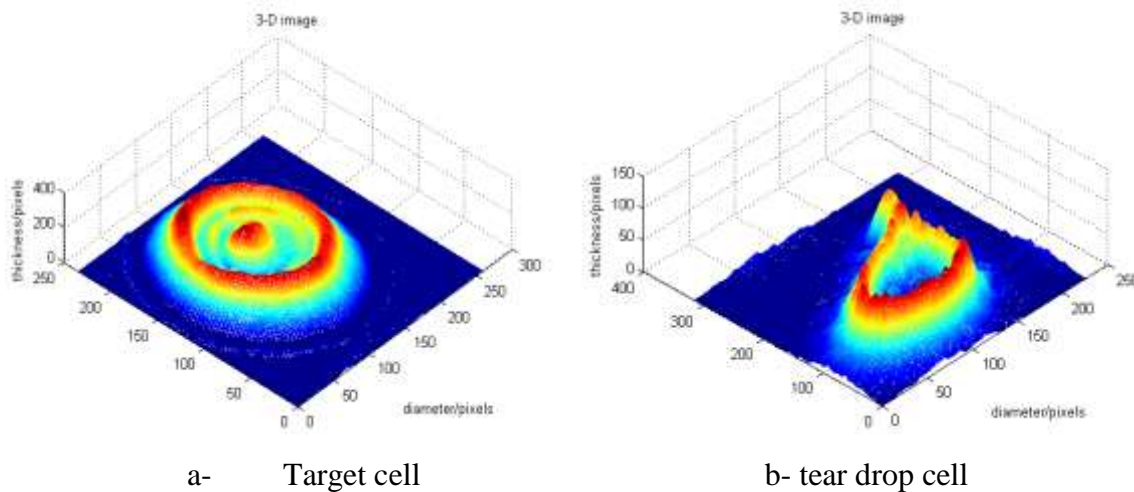


figure 8 . 3D image

The thickness and diameter of the cells is computed from Figure 9.

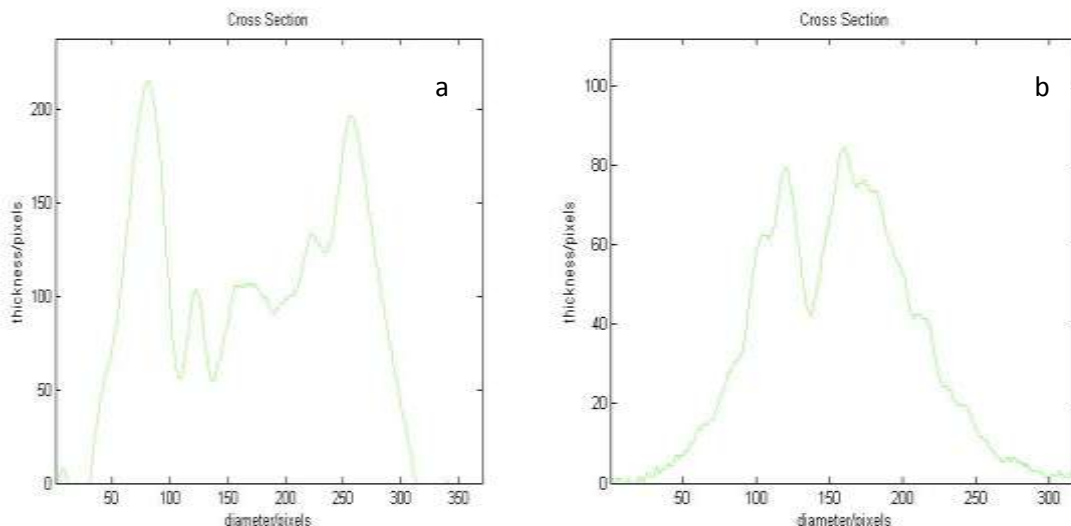


Figure 9. Thickness profile obtained in central cross-section of the cell a-target cell b- tear drop cell. phase profile conveys quantitative information about the physical thickness and index of refraction of cells.

a-target cell We found that Thin Round area of central pigmentation Red cells have an area of increased staining which appears in the area of central pallor thinner than normal with a dark central hemoglobin-containing area gives the cell a target appearance, 8.2 μm in diameter and 3.8 μm in thickness

b- tear drop cell Red cells shaped like a tear drop or pear, 5.5 μm in diameter and 2.2 μm in thickness

A graphic representation of particle size distribution in Figure 9. A histogram, is a graphic representation of a collection of data based on cell size and/or cell number depicting variations in the process. It is sometimes referred to as a frequency of distribution curve. Because graphics can show data in ways that are meaningful and quickly understood, the histogram is a very powerful tool in red cell morphological analysis. It enables one to visualize, analyze, and interpret empirical data that displays morphological changes graphically as points, peaks or valleys, or as a line of frequency curve [12]

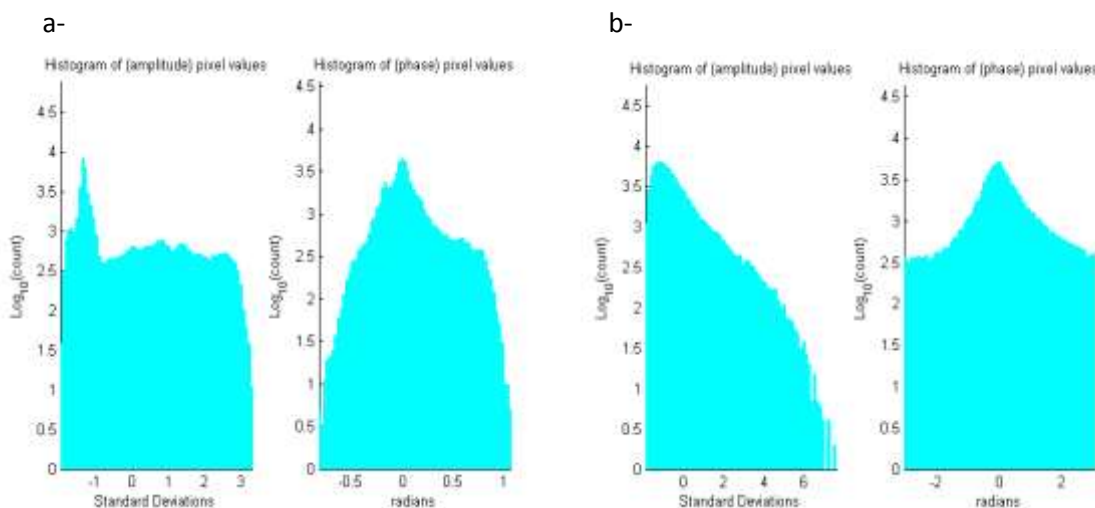


Figure 10. A histogram, as shown in Figure a- target cell and b- tear drop

From diameter, thickness that we calculated it from fig.8 and fig.9 we can determine Refractive indices of individual erythrocytes calculated based on Eq. (12). from h_i is the cellular thickness

$$n_{c,i} = \frac{1}{h_i} \int_0^{h_i} n_{c,i}(z) dz \dots \dots \dots \quad (12)$$

Where z is the axial coordinate, $n_{c,i}(z)$ is the function representing the value of the intracellular refractive index along the cellular thickness h_i [13].the refraction index values for target and tear drop cells are ($n_{\text{target}} = 2.0417$, $n_{\text{tear drop}} = 1.1807$) .

Showed that the Hemoglobin in erythrocytes is dissolved in intracellular fluid supposed to have a higher refractive index than that of water , The membrane of erythrocyte has a slightly higher refractive index than plasma

From the knowledge of refractive indices of individual cells, we can easily translate phase signals from eq. (13) ,phase shift induced on the transmitted wave arises from the difference in refractive index (RI) between the specimen and the surrounding medium $n_m = 1.33$ the refractive index of the plasma , and is proportional to the thickness of the observed transparent specimen. The phase value $\Delta\phi$ can thus be expressed as [14]:

$$\Delta\phi(x, y) = \frac{2\pi}{\lambda} [n_i(x, y) - n_m] h(x, y) \dots \dots \dots \quad (13)$$

where $\lambda = 532 \text{ nm}$, n_i the refractive index of the cell..

The surface areas of individual erythrocytes, which assumes the cell is a truncated cylinder:

$$S_{\text{cell}} = 2\pi r(r + h) \dots \dots \dots \quad (14-a) \quad , \quad r = \frac{d}{2} \dots \dots \dots \quad (14-b)$$

Where r is the radius of RBC and h the thickness and d is the diameter of the cell. [15]

Once the height information is retrieved, are assumed to be cylindrical, leading to the following expression for erythrocyte volume [16] :

$$V_{\text{cell}} = \pi r^2 h \dots \dots \dots \quad (15)$$

Knowing the surface area values for target and tear drop cells are(205.77 , 88.36) μm^2 respectively, and volume values for target and tear drop cells are(205.37 , 55.03) μm^3 respectively, We see that an increase in volume is dependent upon an increase in thickness.

we can calculate parameters such as sphericity (ψ) The sphericity, ψ , It is defined as the ratio between volume of the cell, to the actual surface area of the cell, with values ranging from 0 (for a laminar disk) to 1 for a perfect sphere [17] :

$$\Psi = 4.84 \frac{V^{2/3}}{S_{\text{cell}}} \dots \dots \dots \quad (16)$$

There are more shape of RBCS that had been studied:

Cell name	d μm	h μm	n	OPL (μm)	$\Delta\phi$	S _{cell}	V _{cell}	Ψ
Macrocyte	9.922	3.096	1.6254	0.91	10.79	251.01	239.25	0.743
Target cell	8.202	3.889	2.0417	2.76	32.66	205.77	205.37	0.818
Stchomatocyte	7.938	3.942	2.0695	2.91	34.39	197.18	194.98	0.825
Normocyte	7.408	2.646	1.3891	0.15	1.86	147.70	113.98	0.713
Elliptocyte	6.588	3.836	2.0139	2.62	30.95	171.76	131.17	0.727
Achanthocyte	6.615	2.521	1.3955	0.151	1.784	121.07	86.59	0.782
Tear-drop cell	5.583	2.249	1.1807	0.024	0.283	88.36	55.03	0.792
Bite cell	5.556	3.175	1.6668	1.04	12.36	103.85	76.99	0.843
Spherocyte	5.292	4.233	2.2223	3.76	44.10	114.30	93.06	0.871
Sickle cell	3.969	3.704	1.9446	2.11	24.91	70.89	45.80	0.863

4. Conclusion:

In this paper we design and reconstruction DHM , we have demonstrated a DHM is an efficient and easy to operate interferometric technique ,it can be used in a biological environment as a noninvasive phase contrast microscope to visualize transparent objects such as living cells in a culture. We observed that the Variability in size of RBC in healthy and unhealthy humans RBC may have smaller or bigger diameter than the mean value.

Reference :

- [1] Tristan C., Etienne C., Florian C., Jonas K., Nicolas A., Frédéric M., Pierre M., And Christian D. ,” Automatic Procedure For Aberration Compensation In Digital Holographic Microscopy And Applications To Specimen Shape Compensation” , Applied Optics, Vol. 45, N. 5, 2006.
- [2] C.Depeursinge, “4d Imaging With Nanometer Sensitivity With Digital Holographic Microscopy” ,Advanced Photonics Laboratory
- [3] Jorge G., Wenbo X., Stephan K. J., Peter K.,Manfred H. J., And H. Jürgen Kreuzer,” Digital In-Line Holographic Microscopy” , Applied Optics , Vol. 45, N. 5 , 2006.
- [4] Benjamin R.,Alexander B.Yves E.,Rafi K.,Christian D.,Pierre J. M.,Pierre M.,”Comparative Study Of Human Erythrocytes By Digital Holographic Microscopy, Confocal Microscopy,And Impedance Volume Analyzer”, Wiley Interscience , 2008 .
- [5] Gerhard K. Ackermann And Jürgen Eichler ,“Holography A Practical Approach”, Wiley-Vch.2007.
- [6] P. Harihara,” Basics Of Holography”, Cambridge University Press,2002.
- [7] Myung K. Kim,” Principles And Techniques Of Digital Holographic Microscopy” Spie Digital Library, Vol. 1 ,2010.
- [8]Jonathan Maycock,”Improving Reconstructions Of Digital Holograms”,Vol.2 N. 47 ,2012.
- [9] D. Mas, J. Garcia, C. Ferreira, L. M. Bernardo, and F. Marinho. Fast algorithms for free-space diffraction patterns calculation. Optics Communications, V.164,P.233–245, 1999.
- [10] David Mendlovic, Z. Zalevsky, and N. Konforti. Computation considerations and fast algorithms for calculating the diffraction integral. Journal of Modern Optics, V.44, N.2,P.407–414, 1997.
- [11] T. J. Naughton, J. B. McDonald, and B. Javidi. Efficient compression of Fresnel Fields for Internet transmission of three-dimensional images.Applied Optics, V.42,N.23, P.4758, 2003.
- [12] Benie T. Constantino,”The Red Cell Histogram And The Dimorphic Red Cell Population”, Labmedicine , Vol. 42, N. 5 , 2011.
- [13] Adnan Salih ,And Khawla J .,”Digital In-Line Holography For Blood Cell “,International Journal Of Physical Sciences Vol. 8,N.2, P. 68-72, 16 January, 2013.
- [14] Nicolas Pavillon, Jonas Ku , Corinne Moratal, Pascal Jourdain, Christian Depeursinge, Pierre J.Magistretti, Pierre M. “ Early Cell Death Detection With Digital Holographic Microscopy”, Journal Pone,Vol. 7 ,Issue 1 , No. 2 , January 2012.
- [15] John F. Bertles, “ Sodium Transport Across The Surface Membrane Of Red Blood Cells In Hereditary Spherocytosis”, The University Of Rochester School Of Medicine And Dentistry,1957.
- [16] C.D. Eggleton, A. Vadapalli, T.K. Roy, A.S. Popel, “ Calculations Of Intracapillary Oxygen Tension Distributions In Muscle”, Elsevier Science Inc. ,p. 123–143, 2000.
- [17] Mustafa Aized Hasan Mir, “Quantitative Phase Imaging For Blood Cytometry”, University Of Illinois At Urbana-Champaign, Vol .4, No. 21 ,2010.